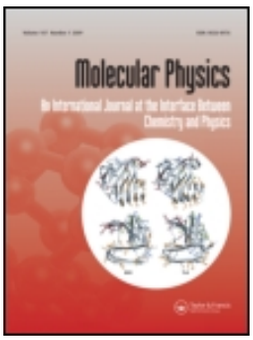

Molecular Physics

ISSN: 0026-8976 (Print) 1362-3028 (Online) Journal homepage: http://www.tandfonline.com/loi/tmph20

Transitions between Hund's coupling cases for the X $^2\Pi$ state of NO

E. KLISCH , S. P. BELOV , R. SCHIEDER , G. WINNEWISSER & ERIC HERBST

To cite this article: E. KLISCH , S. P. BELOV , R. SCHIEDER , G. WINNEWISSER & ERIC HERBST (1999) Transitions between Hund's coupling cases for the X $^2\Pi$ state of NO, Molecular Physics, 97:1-2, 65-79, DOI: 10.1080/00268979909482810

To link to this article: http://dx.doi.org/10.1080/00268979909482810

MOLECULAR PHYSICS, 1999, VOL. 97, NO. 1/2, 65–79

Transitions between Hund's coupling cases for the X $^2\Pi$ state of NO

E. KLISCH, S. P. BELOV†, R. SCHIEDER, G. WINNEWISSER*
Physikalisches Institut, Universität zu Köln, Zülpicher Strasse 77, D-50937 Köln, Germany

and ERIC HERBST
Departments of Physics and Astronomy, The Ohio State University, Columbus, OH 43210 USA

(*Received 10 June 1998; revised version accepted 6 January 1999*)

The submillimetre-wave spectra of $^{14}N^{16}O$, $^{15}N^{16}O$, and $^{14}N^{18}O$ in both the $X^2\Pi_{1/2}$ and $X^2\Pi_{3/2}$ states have been measured in the frequency region 773 GHz to 1.1 THz and assigned. Transitions involving J values between 6.5 and 10.5 have been recorded for the first time. The higher J values display an uncoupling of the electronic spin **S** and the angular momentum **L** from the rotor axis. The **S**-uncoupling leads to an intermediate coupling condition between Hund's case (a) and (b), whereas the **L**-uncoupling causes a coupling scheme intermediate between Hund's case (a) and (d). An improved set of molecular parameters has been obtained for these isotopic species, including magnetic dipole and electric quadrupole constants.

1. Introduction

Nitric oxide, NO, is the only chemically stable open-shell molecule with an unpaired outer electron leading to a $^2\Pi$ ground electronic state. The state is split by an electronic spin–orbit interaction into the lower $X^2\Pi_{1/2}$ and the upper $X^2\Pi_{3/2}$ spin states, which are separated energetically by the value of the fine structure constant $A = 123\,\text{cm}^{-1}$. The analysis of highly precise measurements reveals further insight into the coupling schemes of various angular momenta arising from the interaction between the rotational and the electronic motion of the molecular radical, known as the five Hund's coupling cases labelled (a) through (e) [1]. Heavier hydrides and moderately heavy molecules such as NO approximate Hund's case (a) coupling scheme closely, in which the angular momentum **L** and the electronic spin **S** couple to the intermolecular axis. Deviations from this idealized case occur, however, as a consequence of the interaction of the molecular rotation with the electronic motion and are treated in detail by Herzberg [2]. This interaction leads to a partial **S**-uncoupling as well as an **L**-uncoupling from the molecular axis and is found to depend on the molecular rotational quantum number J.

It is worth noting that in a Hund's case (a) coupling scheme, **L** and **S** are separately decoupled along the internuclear axis. For lower rotational states, the electronic spin **S** is coupled to the molecular axis, as in pure case (a). For higher rotational states, however, **S** slowly uncouples from the molecular axis and eventually couples instead to the angular momentum $\mathbf{N} = \mathbf{\Lambda} + \mathbf{R}$, where **R** is the end-over-end angular momentum of the nuclear frame and $\mathbf{\Lambda}$ is the electronic orbital angular momentum along the nuclear axis, as in pure case (b). This spin uncoupling leads to a change in the effective rotational constants B_{eff} and thus to characteristic shifts involving the two appropriate energy level stacks consisting of the rotational energy levels of the $X^2\Pi_{1/2}$ and $X^2\Pi_{3/2}$ electronic states.

The second effect, the **L**-uncoupling, leads to a splitting of the doubly degenerate electronic orbital states and causes the so-called 'Λ-doubling', as well as a small shift of the levels. The Λ-doubling energies are in general smaller than rotational or fine structure energies, and are therefore seen as small splittings of the rotational levels J belonging to the respective fine structure terms $\Omega = |\Lambda + \Sigma| = 1 - \frac{1}{2} = \frac{1}{2}$ and $\Omega = |\Lambda + \Sigma| = 1 + \frac{1}{2} = \frac{3}{2}$. The uncoupling of **L** from the internuclear axis has the effect of making the molecule intermediate between Hund's case (a) and Hund's case (d), in which **L** couples to the end-over-end rotational motion **R** of the molecule. Both effects, spin-uncoupling and **L**-uncou-

* Author for correspondence.
†On leave of absence from the Microwave Spectroscopy Laboratory, Institute of Applied Physics, Nizhnii Novgorod, Russia 603024.

pling, can be calculated precisely from a direct diagonalization of the complete Hamiltonian. In the present paper we complete the interpretations [1, 2] of spin uncoupling due to linear and nonlinear effects. The linear contribution corresponds to separate uncoupling effects of **S** and **L** to the end-over-end rotational motion **R**, resulting in Hund's case (b) and (d), respectively. The second order effect, which we took into consideration for the first time, pertains to **S**-uncoupling from the rotor axis, which is in effect a coupling from **S** to **L** (case (d)). In other words, a small portion of the spin density does not follow the orientation to coupling case (b), but still interacts with **L** as in case (d) (see 4.1).

The rotational spectrum of NO has provided a valuable test bed for studying these effects. As a consequence of its chemical stability and the relative ease with which it can be handled in a laboratory environment, various aspects of its microwave spectrum were studied as early as 1950 [3]. Since that time, a large number of publications have appeared concerning its structure and spectra in the microwave (see e.g. [4] for a summary), infrared [5], and optical regions of the electromagnetic spectrum.

Although the rotational spectra of NO and its various isotopomers have been studied extensively in the microwave and millimetre-wave regions [3, 5], they have been studied to a much lesser degree in the submillimetre-wave region. Indeed, only some spectral transitions for $^{14}N^{18}O$ and $^{15}N^{16}O$ have been reported at such high frequencies [6]. The observation of spin-uncoupling and **L**-uncoupling requires transitions over a wide range of J values and is aided by the capability of extending microwave spectra into the submillimetre-wave region. In this paper, we report and analyse new terahertz rotational spectra of isotopic NO species in the range 773 GHz–1.1 THz (0.27–0.39 mm). The newly measured high-frequency spectra help to reveal the gradual transition from pure coupling case (a) towards case (b) caused by **S**-uncoupling, as well as towards case (d) caused by **L**-uncoupling. In addition, since NO is an interstellar molecule, these spectral lines are of potential interest for the assignment of unidentified interstellar lines by submillimetre-wave astronomers. Because of the existence of NO in interstellar space, we include a brief discussion of the chemistry of interstellar NO.

2. Experimental

The essential components of the Cologne terahertz spectrometer have been described previously (see e.g. Winnewisser [7]). The tunable source is a frequency- and phase-stabilized backward wave oscillator (BWO) supplied by the ISTOK Research and Production Company, Moscow region, Russia. Its high frequency output is phase-locked via an off-axis harmonic mixer system to a KVARZ frequency synthesizer operating in the 78–118 GHz region, which is fed by a 5 MHz reference signal from a rubidium atomic clock. The major portion of the BWO radiation (typically 1–3 mW) is focused through a free space absorption cell 4.5 m in length, and then detected with a magnetically tuned, He-cooled InSb hot-electron bolometer with optimized sensitivity in the 1–2 THz region. The accuracy of the present measurements of single unblended lines is estimated to be better than 10 kHz, as monitored by reference measurements on CO [8]. The spectra were recorded at pressures between 15 and 40 μbar.

The isotopomer $^{14}N^{16}O$ was measured in its natural abundance of 99.4%; $^{15}N^{16}O$ and $^{14}N^{18}O$, however, possess natural abundances of only 0.37% and 0.20%, respectively. For these isotopomers, therefore, we used isotopically enriched samples for the present measurements. Enriched samples of $^{15}N^{16}O$ were synthesized from ^{15}N-substituted nitric acid, HNO_3, sulphuric acid, H_2SO_4, and mercury, Hg, by means of the reaction [9]:

$$2HNO_3 + 6Hg + 3H_2SO_4 \rightarrow 2NO + 3Hg_2SO_4 + 4H_2O. \quad (1)$$

The result was 15% enriched $^{15}N^{16}O$. The $^{14}N^{18}O$ sample was produced by the same reaction, with ^{18}O-enriched nitric acid, HNO_3, obtained by the reaction of ^{18}O-substituted water with N_2O_4:

$$H_2O + N_2O_4 \rightarrow HNO_2 + HNO_3. \quad (2)$$

The resulting relative abundance of $^{14}N^{18}O$ was 82%.

3. Rotational spectrum

The observed pure rotational spectral lines of NO are divided into two sets of transitions arising from the $^2\Pi_{1/2}$ and $^2\Pi_{3/2}$ electronic ground state energy levels. The latter state is energetically about 123 cm^{-1} higher than the $^2\Pi_{1/2}$ state; the order is known as 'regular' since the energies of the two states $\Omega = \frac{1}{2}$ and $\Omega = \frac{3}{2}$ are in the order of their increasing Ω values. This order is associated with a positive spin–orbit constant A, which is equal to the energy separation of the two spin–orbit-split states. As opposed to NO, the radical SH exhibits the inverted case; i.e. the $^2\Pi_{3/2}$ spin state is lower the $^2\Pi_{1/2}$ state. This order is associated with a negative spin–orbit constant, in this case $A = -375\,cm^{-1}$. For NO, the energy difference between the $^2\Pi_{1/2}$ and $^2\Pi_{3/2}$ electronic states has been measured directly by Saleck *et al.* [5] in the far infrared region by observing the $^2\Pi_{3/2} \leftarrow {}^2\Pi_{1/2}$ transitions with the Giessen Fourier transform spectrometer. The analysis of these spectra allowed the accurate determination of the spin–orbit coupling constant ($A = 123.1540(15)\,cm^{-1}$), together with the electron spin–rotation constant γ, which is fully correlated with D_A, the centrifugal distortion

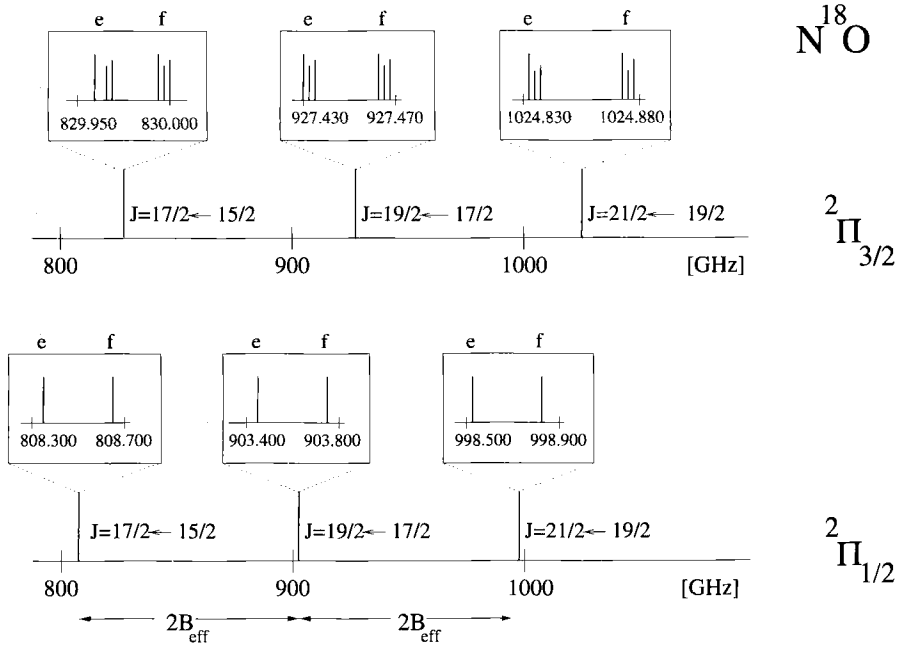

Figure 1. A stick diagram of the newly measured $N^{18}O$ pure rotational spectrum near 1 THz. The Λ-type doubling is depicted for both the $^2\Pi_{1/2}$ and $^2\Pi_{3/2}$ spin–orbit split substates as e and f components, while the hyperfine structure is shown only for the latter.

term of A. Although most other molecular parameters, such as the rotational constant, B, and the centrifugal distortion constant, D, the Λ-doubling constants p and q with their associated centrifugal distortion contributions, and the various hyperfine constants have already been determined to high accuracy, the effects of spin **S**- and **L**-uncoupling associated with the higher rotational transitions remain an intriguing question.

Figure 1 presents a stick diagram of the newly measured $N^{18}O$ pure rotational spectrum near 1 THz, which consists of two sets of rotational lines associated with the $X^2\Pi_{1/2}$ and $X^2\Pi_{3/2}$ spin states. The approximate spacing between successive rotational lines in each spin state series is determined by the effective rotational constant. For the $X^2\Pi_{1/2}$ state, the effective rotational constant is [10],

$$B_{\text{eff}} = B_v\left(1 - \frac{B_v}{AA} + \cdots\right), \qquad (3)$$

whereas for the $X^2\Pi_{3/2}$ state, the effective rotational constant is

$$B_{\text{eff}} = B_v\left(1 + \frac{B_v}{AA} + \cdots\right), \qquad (4)$$

where the positive value of A $(=1)$ is chosen. Consequently, the $^2\Pi_{3/2}$ state possesses a slightly wider rotational spacing than the $^2\Pi_{1/2}$ state. The correction term B_v/A is 0.0138 for NO and 0.0131 for $N\,^{18}O$, which is in good agreement with the value 0.014 given by Gordy and Cook [10]. Each rotational energy level is split by the Λ-doubling into two levels, labelled according to the symmetry e and f introduced by Brown *et al.* [11]. The allowed transitions are e ← e and f ← f, so that each rotational transition is split into two components e and f.

The effect of Λ-doubling is typically greater for the $X^2\Pi_{1/2}$ electronic spin state than for the $X^2\Pi_{3/2}$ state. The $J = 17/2 \leftarrow 15/2$ rotational transition of $^{14}N^{16}O$, for example, exhibits a frequency splitting of 326 MHz for the $^2\Pi_{1/2}$, but only 42 MHz for the $^2\Pi_{3/2}$ state. Associated with the splittings are the Λ-doubling constants p and q (often denoted by other letters). As can be seen from the Hamiltonian matrix with case (a) basis, discussed in the next section, p and, to a lesser extent, q determine the Λ-doublet splitting for the $X^2\Pi_{1/2}$ electronic state, but for the $X^2\Pi_{3/2}$ state p is not relevant and q is present only in matrix elements off-diagonal in Ω. These provide small contributions for the $X^2\Pi_{3/2}$ state after diagonalization. The J dependence of the terms multiplying p and q after diagonalization are such that the Λ-splitting increases for the $X^2\Pi_{1/2}$ spin state approximately linearly with J, whereas for the $X^2\Pi_{3/2}$ state, the doubling increases more rapidly, approximately with J^3. NO deviates markedly from a pure Hund's case (a) representation. The difference is caused mainly by **S**-uncoupling, which can be said to transfer some of the large Λ-doublet splitting of the $X^2\Pi_{1/2}$ electronic state to the $X^2\Pi_{3/2}$ state.

Each of the Λ-doublet-split transitions is further split by the effects of hyperfine splitting, which in the case of NO arises from three different contributions. In order of descending magnitude these are: the magnetic dipole contributions a, b, c, d, the electric quadrupole terms eQq_1 (diagonal) and eQq_2 (off-diagonal), and the contributions from the nuclear spin–rotation C_I and $C_{I'}$. The hyperfine structure of the $X^2\Pi_{1/2}$ state is often too small to be resolved for NO, and thus the Λ-splitting

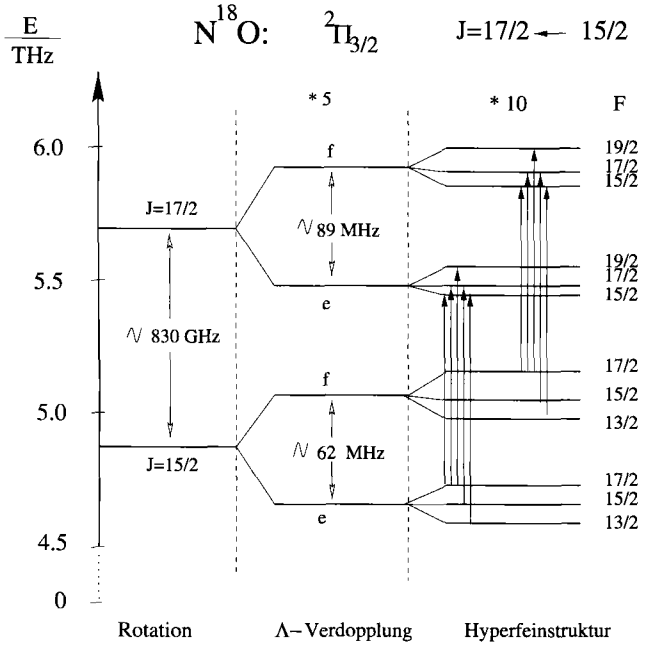

Figure 2. Rotational energy levels relevant to the $J = 17/2 \leftarrow 15/2\,^2\Pi_{3/2}$ transition of $N^{18}O$. Both the Λ-type doubling and the hyperfine splittings are depicted.

is left essentially unaltered. However, for the $X^2\Pi_{3/2}$ state a clearly detectable hyperfine pattern results. Each Λ-transition consists of five hyperfine components with varying intensities and a frequency spread of about 20 MHz. In the inserts of figure 1 only the three most intense of the five hyperfine components are drawn. The appropriate energy level scheme for the $J = 17/2 \leftarrow 15/2$ $X^2\Pi_{3/2}$ transition is depicted in figure 2 for the $N^{18}O$ isotopomer, while figure 3 presents a recording of the same transition in a scan covering the frequency range from 829.950 to 830.000 GHz.

In total, we have measured 74 rotational transitions of NO and its isotopomers between 770 GHz and 1.1 THz. Of these, 14 transitions belong to ^{15}NO, 36 to $N^{18}O$, and 24 to $^{14}N^{16}O$. Table 1 lists the observed transitions together with their relative intensities, residuals (observed–calculated frequencies), upper energy levels E′ of the appropriate transitions, and absorption coefficients α_{max}. Three medium J lines of $^{14}N^{16}O$ from the far-infrared FT data published by Saleck *et al.* [4] have been remeasured in the present work and are quoted in table 1. The FT measurements agree with our more precise data to within 1 MHz, a level of agreement similar to that found in a comparison of H_2S data measured in the two laboratories [12].

It should be noted that hyperfine structure transitions of various intensities have been observed. Some hyperfine structure transitions with very small absorption coefficients down to $\alpha = 2.2 \times 10^{-8}\,cm^{-1}$ have been detected by long integration times; these provide an excellent demonstration of the sensitivity of our spectrometer system in the 1 THz region. Because the absorption coefficient α_{max} depends on the isotopic concentration, $^{14}N^{16}O$ measured in natural abundance

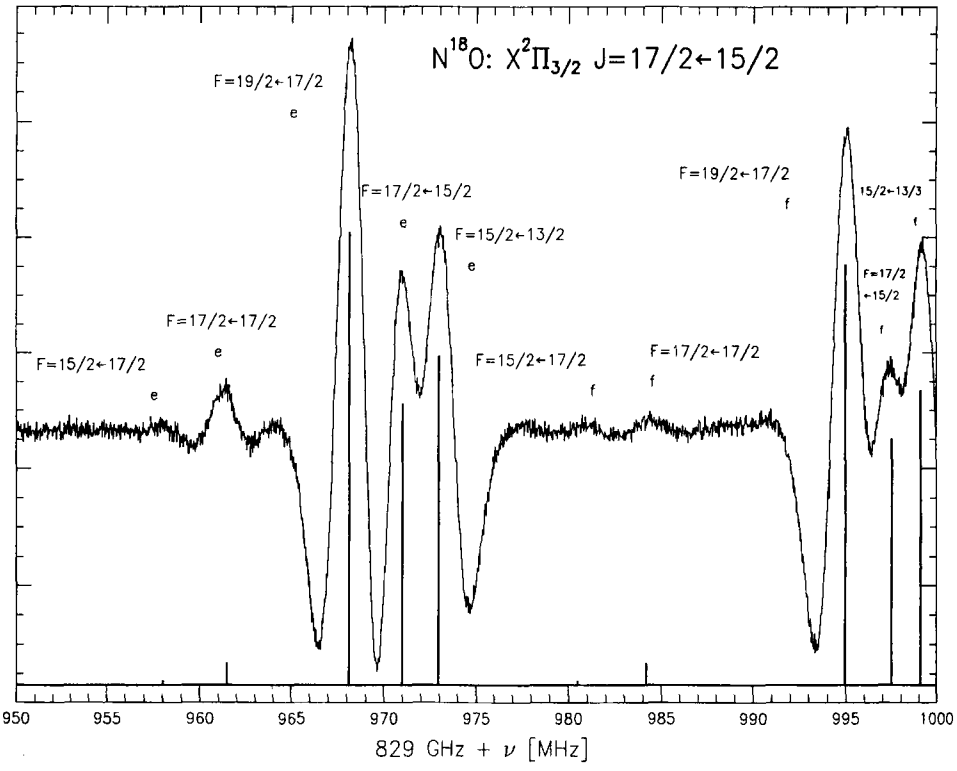

Figure 3. Recording of the $J = 17/2 \leftarrow 15/2$ $^2\Pi_{3/2}$ transition of $N^{18}O$ at 829–830 GHz. The Λ-type doubling and the hyperfine splittings are assigned.

Table 1. Observed rotational transitions of $^{14}N^{16}O$, and $^{15}N^{16}O$ and $^{14}N^{18}O$.

$J'_{F'} \leftarrow J''_{F''}$ [a]	Ω' [b]	Sym.' [b]	ν_{exp} [c]/[MHz]	rel. Int.	Residual/[MHz]	$E'/[cm^{-1}]$	$\alpha/[cm^{-1}]$ [d]
$^{14}N^{16}O$							
$7.5_{7.5} \leftarrow 6.5_{7.5}$	1.5	e	773 016.806 (120)	0.006	−0.060	228.084	0.000 008 634
$7.5_{6.5} \leftarrow 6.5_{6.5}$	1.5	e	773 020.428 (120)	0.006	−0.057	228.084	0.000 008 634
$7.5_{8.5} \leftarrow 6.5_{7.5}$	1.5	e	773 026.021 (100)	0.375	−0.066	228.084	0.000 546 357
$7.5_{7.5} \leftarrow 6.5_{6.5}$	1.5	e	773 029.169 (100)	0.327	−0.070	227.084	0.000 477 021
$7.5_{6.5} \leftarrow 6.5_{6.5}$	1.5	e	773 031.754 (110)	0.286	+0.109	228.084	0.000 416 278
$7.5_{7.5} \leftarrow 6.5_{7.5}$	1.5	f	773 038.410 (130)	0.006	+0.033	228.086	0.000 008 634
$7.5_{6.5} \leftarrow 6.5_{6.5}$	1.5	f	773 045.323 (120)	0.006	−0.103	228.086	0.000 008 634
$7.5_{8.5} \leftarrow 6.5_{7.5}$	1.5	f	773 050.731 (100)	0.375	−0.128	228.087	0.000 546 391
$7.5_{7.5} \leftarrow 6.5_{6.5}$	1.5	f	773 053.434 (100)	0.327	−0.012	228.086	0.000 477 050
$7.5_{6.5} \leftarrow 6.5_{5.5}$	1.5	f	773 055.891 (110)	0.286	+0.120	228.086	0.000 416 303
$8.5 \leftarrow 7.5$	0.5	e	851 913.248 (100)		+0.031	133.709	0.001 003 426
$8.5_{7.5} \leftarrow 7.5_{7.5}$	0.5	e	851 957.265 (140)	0.005	−0.134	133.710	0.000 014 019
$8.5_{8.5} \leftarrow 7.8_{8.5}$	0.5	e	851 959.528 (140)	0.005	+0.065	133.709	0.000 014 019
$8.5_{8.5} \leftarrow 7.5_{8.5}$	0.5	f	852 169.502 (120)	0.005	+0.016	133.812	0.000 014 026
$8.5_{7.5} \leftarrow 7.5_{7.5}$	0.5	f	852 176.948 (120)	0.005	+0.002	133.810	0.000 014 026
$8.5 \leftarrow 7.5$	0.5	f	852 239.423 (100)		+0.045	133.812	0.001 004 167
$8.5 \leftarrow 7.5$	1.5	e	875 920.944 (400)		−0.488	257.302	0.000 008 326
$8.5_{9.5} \leftarrow 7.5_{8.5}$	1.5	e	875 927.543 (100)	0.370	−0.184	257.302	0.000 668 407
$8.5_{8.5} \leftarrow 7.5_{7.5}$	1.5	e	875 930.629 (150)	0.329	+0.293	257.302	0.000 593 244
$8.5_{7.5} \leftarrow 7.5_{6.5}$	1.5	e	875 932.382 (120)	0.292	+0.017	257.302	0.000 526 376
$8.5_{8.5} \leftarrow 7.5_{8.5}$	1.5	f	875 948.625 (150)	0.005	−0.019	257.305	0.000 008 327
$8.5_{9.5} \leftarrow 7.5_{8.5}$	1.5	f	875 959.028 (100)	0.370	−0.076	257.306	0.000 668 453
$8.5 \leftarrow 7.5$	1.5	f	875 962.997 (400)		−0.137	257.305	0.000 559 848
$9.5 \leftarrow 8.5$	0.5	e	952 145.425 (150)		+0.021	165.469	0.001 178 936
$9.5_{9.5} \leftarrow 8.5_{9.5}$	0.5	f	952 395.069 (80)	0.004	+0.007	165.583	0.000 013 167
$9.5_{8.5} \leftarrow 8.5_{8.5}$	0.5	f	952 401.336 (90)	0.004	−0.002	165.581	0.000 013 167
$9.5 \leftarrow 8.5$	0.5	f	952 464.194 (120)		−0.044	165.583	0.001 179 693
$10.5 \leftarrow 9.5$	0.5	e	1 052 370.117 (120)		+0.023	200.573	0.001 319 873
$10.5 \leftarrow 9.5$	0.5	e	1 052 414.790 (200)	0.003	−0.080	200.574	0.000 012 046
$10.5_{9.5} \leftarrow 9.5_{10.5}$	0.5	e	1 052 457.636 (300)†	0.000	—	200.574	0.000 000 027
$10.5_{10.5} \leftarrow 9.5_{10.5}$	0.5	f	1 052 612.439 (120)	0.003	−0.002	200.696	0.000 012 050
$10.5_{9.5} \leftarrow 9.5_{9.5}$	0.5	f	1 052 617.748 (120)	0.003	+0.010	200.694	0.000 012 050
$10.5 \leftarrow 9.5$	0.5	f	1 052 680.969 (120)		−0.019	200.696	0.001 320 617
$10.5 \leftarrow 9.5$	1.5	e	1 081 588.326 (500)		−0.214	326.033	0.000 782 934
$^{15}N^{16}O$							
$8.5 \leftarrow 7.5$	0.5	e	822 210.888 (90)		+0.081	129.049	0.000 139 677
$8.5 \leftarrow 7.5$	0.5	f	822 525.781 (200)		+0.105	129.149	0.000 139 780
$9.5 \leftarrow 8.5$	0.5	e	918 942.915 (120)		+0.126	159.702	0.000 164 867
$9.5 \leftarrow 8.5$	0.5	f	919 251.379 (110)		+0.074	159.812	0.000 164 973
$9.5_9 \leftarrow 8.5_8$	1.5	e	943 759.876 (100)	0.472	−0.052	283.980	0.000 092 475
$9.5_{10} \leftarrow 8.5_9$	1.5	e	943 762.626 (100)	0.525	−0.079	283.980	0.000 102 811
$9.5_9 \leftarrow 8.5_8$	1.5	f	943 794.388 (100)	0.472	−0.171	283.984	0.000 053 915
$9.5_{10} \leftarrow 8.5_9$	1.5	f	943 796.917 (100)	0.525	+0.092	283.984	0.000 102 818
$10.5 \leftarrow 9.5$	0.5	e	1 015 666.406 (180)		+0.238	193.581	0.000 185 595
$10.5 \leftarrow 9.5$	0.5	f	1 015 967.938 (80)		+0.150	193.701	0.000 185 701
$10.5_{10} \leftarrow 9.5_9$	1.5	e	1 042 872.142 (120)	0.475	−0.124	318.766	0.000 104 593
$10.5_{11} \leftarrow 9.5_{10}$	1.5	e	1 042 874.862 (120)	0.523	+0.150	318.766	0.000 115 102
$10.5_{10} \leftarrow 9.5_9$	1.5	f	1 042 913.916 (180)	0.475	−0.043	318.772	0.000 104 601
$10.5_{11} \leftarrow 9.5_{10}$	1.5	f	1 042 915.656 (180)	0.523	−0.211	318.772	0.000 115 111
$^{14}N^{18}O$							
$8.5 \leftarrow 7.5$	0.5	e	808 338.541 (180)		+0.205	126.873	0.000 712 014
$8.5_{7.5} \leftarrow 7.5_{7.5}$	0.5	e	808 382.953 (180)	0.005	+0.079	126.874	0.000 009 945

(*continued*)

Table 1. *Continued*

$J'_{F'} \leftarrow J''_{F''}$ [a]	Ω' [b]	Sym.' [b]	ν_{exp} [c]/[MHz]	rel. Int.	Residual/[MHz]	$E'/[cm^{-1}]$	$\alpha/[cm^{-1}]$ [d]
$8.5_{8.5} \leftarrow 7.5_{8.5}$	0.5	e	808 385.303 (180)	0.005	+0.264	126.872	0.000 009 945
$8.5_{8.5} \leftarrow 7.5_{8.5}$	0.5	f	808 580.628 (180)	0.005	−0.021	126.970	0.000 009 953
$8.5_{7.5} \leftarrow 7.5_{7.5}$	0.5	f	808 588.159 (180)	0.005	−0.016	126.968	0.000 009 953
$8.5 \leftarrow 7.5$	0.5	f	808 650.422 (180)		+0.195	126.970	0.000 712 544
$8.5_{7.5} \leftarrow 7.5_{8.5}$	1.5	e	829 958.072 (400)†	0.000	—	250.259	0.000 000 020
$8.5_{8.5} \leftarrow 7.5_{8.5}$	1.5	e	829 961.354 (180)	0.005	−0.041	250.259	0.000 005 888
$8.5_{9.5} \leftarrow 7.5_{8.5}$	1.5	e	829 968.269 (70)	0.370	−0.136	250.259	0.000 472 699
$8.5_{8.5} \leftarrow 7.5_{7.5}$	1.5	e	829 971.093 (100)	0.292	+0.123	250.259	0.000 419 544
$8.5_{7.5} \leftarrow 7.5_{6.5}$	1.5	e	829 973.062 (80)	0.329	+0.098	250.259	0.000 372 255
$8.5_{7.5} \leftarrow 7.5_{8.5}$	1.5	f	829 981.100 (400)†	0.000	—	250.259	0.000 000 020
$8.5_{8.5} \leftarrow 7.5_{8.5}$	1.5	f	829 984.552 (200)	0.005	−0.181	250.262	0.000 005 889
$9.5_{8.5} \leftarrow 8.5_{7.5}$	1.5	f	829 995.161 (100)	0.370	−0.151	250.262	0.000 472 729
$8.5_{8.5} \leftarrow 7.5_{7.5}$	1.5	f	829 997.481 (150)	0.292	+0.149	250.262	0.000 419 569
$8.5_{7.5} \leftarrow 7.5_{6.5}$	1.5	f	829 999.239 (180)	0.329	+0.003	250.262	0.000 372 277
$9.5 \leftarrow 8.5$	0.5	e	903 436.474 (180)		+0.073	157.008	0.000 843 670
$9.5 \leftarrow 8.5$	0.5	e	903 481.825 (500)	0.004	+0.128	157.009	0.000 009 419
$9.5_{9.5} \leftarrow 8.5_{9.5}$	0.5	f	903 672.948 (120)	0.004	−0.029	157.116	0.000 009 423
$9.5_{8.5} \leftarrow 8.5_{8.5}$	0.5	f	903 679.312 (120)	0.004	−0.009	157.114	0.000 009 423
$9.5 \leftarrow 8.5$	0.5	f	903 741.938 (200)		+0.250	157.116	0.000 844 218
$9.5_{10.5} \leftarrow 8.5_{9.5}$	1.5	e	927 431.014 (80)	0.367	−0.169	281.195	0.000 553 136
$9.5_{9.5} \leftarrow 8.5_{8.5}$	1.5	e	927 433.514 (120)	0.330	+0.135	281.195	0.000 497 282
$9.5_{8.5} \leftarrow 8.5_{7.5}$	1.5	e	927 435.089 (100)	0.296	−0.018	281.195	0.000 446 982
$9.5_{9.5} \leftarrow 8.5_{9.5}$	1.5	f	927 455.478 (120)	0.004	+0.021	281.199	0.000 005 572
$9.5_{10.5} \leftarrow 8.5_{9.5}$	1.5	f	927 464.525 (120)	0.367	+0.114	281.199	0.000 553 174
$9.5 \leftarrow 8.5$	1.5	f	927 467.146 (500)	0.330	+0.617	281.199	0.000 472 164
$10.5 \leftarrow 9.5$	0.5	e	998 525.410 (180)		−0.161	190.315	0.000 953 375
$10.5 \leftarrow 9.5$	0.5	e	998 570.458 (200)	0.003	−0.074	190.316	0.000 008 701
$10.5_{10.5} \leftarrow 9.5_{10.5}$	0.5	f	998 755.707 (130)	0.003	+0.057	190.433	0.000 008 704
$10.5_{9.5} \leftarrow 9.5_{9.5}$	0.5	f	998 761.200 (130)	0.003	+0.171	190.431	0.000 008 704
$10.5 \leftarrow 9.5$	0.5	f	998 824.026 (130)		+0.185	190.433	0.000 953 920
$10.5_{11.5} \leftarrow 9.5_{10.5}$	1.5	e	1 024 835.710 (120)	0.364	+0.044	315.380	0.000 618 669
$10.5 \leftarrow 9.5$	1.5	e	1 024 838.582 (500)		+0.437	315.380	0.000 536 189
$10.5_{11.5} \leftarrow 9.5_{10.5}$	1.5	f	1 024 875.690 (120)	0.364	−0.076	315.380	0.000 618 716
$10.5_{10.5} \leftarrow 9.5_{9.5}$	1.5	f	1 024 877.697 (200)	0.330	−0.185	315.383	0.000 562 013

[a] For transitions where the hyperfine structure is not resolved, the hyperfine quantum numbers F and F' are omitted.
[b] $\Omega' = \Omega''$, corresponding to the selection rules of electric dipole transitions.
[c] Numbers in parentheses denote the estimated uncertainties of measured frequencies in units of the last quoted digit. Uncertainties are 1σ.
[d] The absorption coefficient was calculated to room temperature (300 K).
† Not included in the fit.

and $^{14}N^{18}O$ observed in an isotopically enriched sample with a relative abundance of 84% are both well suited to the search for transitions possessing very small intensities, while the $^{15}N^{16}O$ isotopomer with a maximum enriched relative abundance of only 15% is not.

4. Theory and analysis

In our analysis, we have included both our new NO measurements and much of the relevant data on NO that is available in the literature, which includes: (i) the Λ-type doubling data of Meerts and Dymanus [13]; (ii) the far infrared Fourier transform high J pure rotational transitions of $^{14}N^{16}O$ of Meerts [14]; (iii) the millimetre and submillimetre transitions of the isotopomers ^{15}NO and $N^{18}O$ [4] and the Fourier transform data [5] of Saleck *et al.* All lines were fitted to an effective Hamiltonian of the form

$$H_{eff} = H_{so} + H_{sr} + H_{rot} + H_{cd} + H_{\Lambda d} + H_{hfs}, \quad (5)$$

where the subscripts so, sr, rot, cd, Λd, and hfs refer to spin–orbit, spin–rotation, rotational motion, centrifugal distortion, Λ-type doubling, and hyperfine contributions, respectively. By applying a nonlinear least squares fit to the entire data set, we obtained the molecular parameters summarized in table 2.

Table 2. Molecular parameters of NO and its isotopomeres in the ground state.

Parameter	NO	^{15}NO	N^{18}O	Unit
A	3.692 064 2 (28)	3.691 683[a]	3.691 713[a]	THz
D_A	7.133 6 (29)	5.113 (11)	4.9451 (28)	MHz
B	50 847.801 6 (15)	49 050.534 3 (82)	48 211.777 2 (22)	MHz
D	164.099 0 (82)	152.715 (56)	147.608 (53)	kHz
H	682 (41)	—	594 (37)	mHz
p	350.440 80 (16)	337.959 91 (41)	332.207 (33)	MHz
D_p	305 (64)	170 (32)	—	Hz
q	2.804 324 (84)	2.641 46 (16)	2.518 (20)	MHz
D_q	43.71 (49)	38.3 (23)	76 (14)	Hz
a	84.215 3 (11)	−118.143 0 (30)	84.225 (31)	MHz
b	41.904 9 (75)	−59.025 (15)	42.05 (34)	MHz
c	−58.795 0 (75)	82.726 (13)	−58.92 (34)	MGz
d	112.597 38 (29)	−157.947 84 (70)	112.576 (21)	MHz
D_d	−457 (46)	−452 (37)	—	Hz
C_I	12.45 (10)	−16.24 (20)	−9.3 (22)	kKz
$C_{I'}$	1.24 (55)	−1.34 (70)	—	kHz
eQq_1	−1.857 49 (74)	—	−1.839 (37)	MHz
eQq_2	23.049 (18)	—	23.30 (67)	MHz

[a] Fixed to the value given by Amiot [30].

The Hamiltonian was evaluated in a parity basis

$$|n^2\Pi_{|\Omega|}vJ\pm\rangle = 2^{-1/2}\{|nvJ\Omega S\Lambda\Sigma\rangle \pm (-)^{J-S}|nvJ(-\Omega)S(-\Lambda)(-\Sigma)\rangle\}, \quad (6)$$

representing Hund's case (a) [15]. For the hyperfine analysis, the basis was extended to include the total angular momentum quantum number F, where

$$\mathbf{F} = \mathbf{I} + \mathbf{J}; \quad (7)$$

and $I = 1/2$ or 1 depending on the nitrogen isotope. In the extended basis, the Hamiltonian can be represented by a 2×2 matrix:

$$\begin{pmatrix} \langle {}^2\Pi_{\frac{1}{2}} J' \tfrac{1}{2} F \pm |\hat{H}_{\text{eff}}|^2\Pi_{\frac{1}{2}} J \tfrac{1}{2} F\pm\rangle & \\ & \langle {}^2\Pi_{\frac{3}{2}} J' \tfrac{1}{2} F \pm |\hat{H}_{\text{eff}}|^2\Pi_{\frac{1}{2}} J \tfrac{1}{2} F\pm\rangle \\ \langle {}^2\Pi_{\frac{1}{2}} J' \tfrac{1}{2} F \pm |\hat{H}_{\text{eff}}|^2\Pi_{\frac{3}{2}} J \tfrac{1}{2} F\pm\rangle & \\ & \langle {}^2\Pi_{\frac{3}{2}} J' \tfrac{1}{2} F \pm |\hat{H}_{\text{eff}}|^2\Pi_{\frac{3}{2}} J \tfrac{1}{2} F\pm\rangle \end{pmatrix}$$

where, as an example, I has been set equal to 1/2.

The rotational contribution to the Hamiltonian has matrix elements both on- and off-diagonal in spin–orbit state in the case (a) parity basis; the latter can be regarded as the cause of the **S**-uncoupling (see appendix). The on-diagonal elements contain the rotational constant B as well as the fine structure constant A while the off-diagonal elements contain the rotational constant B only. As the quantum number J increases, the relative importance of the off-diagonal elements increases and the degree of **S**-uncoupling increases. Eventually, **S** is totally decoupled from the intermolecular axis and a Hund's case (b) representation is appropriate, in which **S** is coupled to the sum of the end-over-end rotation of the molecule and the electronic orbital angular momentum along the internuclear axis ($\mathbf{N} = \Lambda + \mathbf{R}$). To determine the size of the **S**-uncoupling as a function of J with our Hund's case (a) basis, we calculated rotational–spin–orbit energies with and without off-diagonal elements, and took the difference ΔE between them as a measure of the **S**-uncoupling. This mathematical procedure goes along with an extensive discussion of Carrington [16] who focuses the reader's attention on the magnitudes of the rotational constant B and the effective spin–orbit coupling A in order to give a conception of the size of the **S**-uncoupling. In his expansion of the Hamiltonian in terms of the molecule-fixed axes, the uncoupling part is described in three terms:

$$\tilde{H} = -2B\{J_xL_x + J_yL_y\} + (A+2B)\{L_xS_x + L_yS_y\} - 2B\{J_xS_x + J_yS_y\}, \quad (8)$$

which indicates admixtures of the spin **S** and the electronic angular momentum **L** with the total angular momentum **J** and therefore leads to uncoupling effects. The above representation of $\tilde{H}$ can be derived from the use of the defined operators

$$T_\pm = T_x \pm iT_y \quad (9)$$

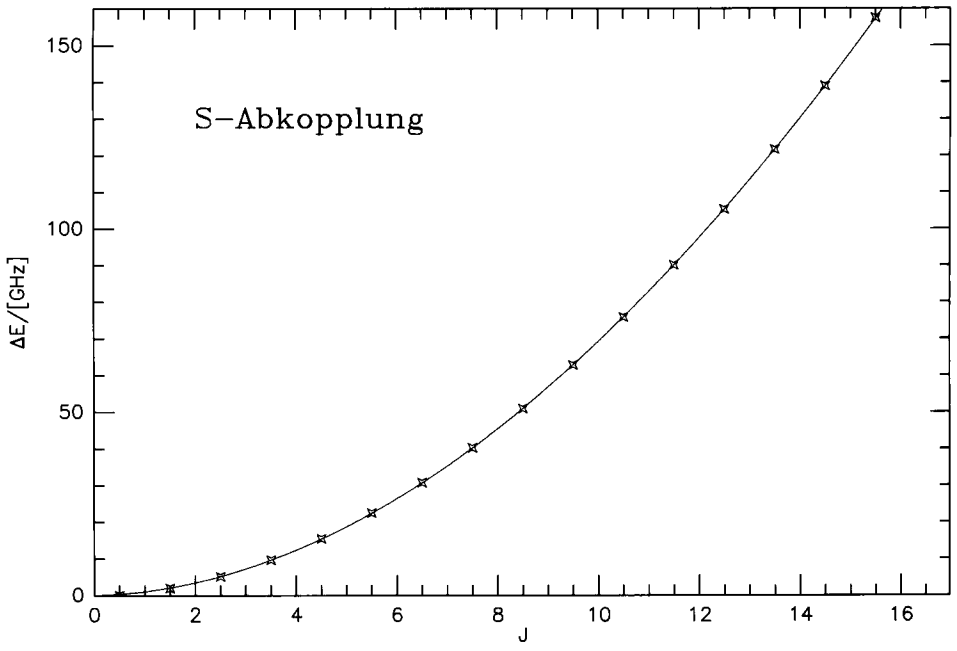

Figure 4. S-uncoupling in $N^{18}O$ is plotted versus J.

for the angular momenta **S**, **L** and **J**. Since the spin–orbit coupling constant A and the rotational parameter B determine $\tilde{H}$ our procedure is in line with the interpretation of Carrington [16]. Moreover we give a semi-classical justification for the rotational motion B leading to spin uncoupling (see appendix). The Hamiltonian we used to determine the **S**-uncoupling includes the rotational motion as well as the spin–orbit interaction in accordance with the expression quoted in equation (8). The explicit matrix elements are shown below:

$$\hat{H} = \left\{ \tfrac{1}{2}A \begin{pmatrix} -1 & 0 \\ 0 & 1 \end{pmatrix} + B \begin{pmatrix} J^2+J+\frac{1}{4} & -(J^2+J-\frac{3}{4})^{1/2} \\ -(J^2+J-\frac{3}{4})^{1/2} & J^2+J-\frac{7}{4} \end{pmatrix} \right\} \delta_{J',J}. \tag{10}$$

In figure 4, ΔE, plotted for $N^{18}O$ shows an approximate quadratic dependence on J and ranges in size up to $\approx$ 150 GHz for $J = 15.5$. The criterion for a good case (a) molecule, for which equation (6) is applicable, is [11]

$$2JB \ll |\Lambda A|, \tag{11}$$

which is characterized by the parameters B and A, as chosen by Carrington (equation (8)) and the authors (equation (10)). For NO, $2JB$ amounts to 26% of the right side when $J = 8.5$, which indicates an admixing of Hund's case (b) wave functions, resulting in an intermediate uncoupling of the electron spin.

4.1. *Fine structure*

Typically for Hund's case (a) molecules, the energy splitting of the Λ-type doublets is different for the two spin states, $^2\Pi_{1/2}$ and $^2\Pi_{3/2}$. The $^2\Pi_{1/2}$ state displays the larger splitting, which results from the explicit matrix elements of the Hamiltonian:

$$(\hat{H}_{\Lambda D}) = \mp\{p + D_p J(J+1)\} \begin{pmatrix} \frac{1}{2}(J+\frac{1}{2}) & 0 \\ 0 & 0 \end{pmatrix} \mp \{q + D_q J(J+1)\} \times \begin{pmatrix} J+\frac{1}{2} & -\frac{1}{2}(J+\frac{1}{2})X^{1/2} \\ -\frac{1}{2}(J+\frac{1}{2})X^{1/2} & 0 \end{pmatrix}, \tag{12}$$

where $X = J(J+1) - \frac{3}{4}$ and $\pm$ refers to the parity function. The $^2\Pi_{1/2}$ state splitting is determined by the Λ-type doubling parameters p and q, while the contributions referring to the $^2\Pi_{3/2}$ state are only dependent on the off-diagonal elements in q.

The analysis of Λ-type doubling in terms of a 2×2 matrix is a simplification of the actual situation, in which matrix elements between the Ω components of the $^2\Pi$ state and all $^2\Sigma$ states cause the effect. These matrix elements, connecting states of different Λ ($\Lambda = -1, 0, +1$), have the effect of causing the so-called **L**-uncoupling from the internuclear axis. Eventually, as J increases, **L** is more profitably coupled to the end-over-end rotation **R** of the molecule, a situation known as Hund's case (d). Since it is difficult to isolate perturbing $^2\Sigma$ states, a perturbation treatment first presented by van Vleck [17] is normally used. The $(\hat{H}_{\Lambda D})$ matrix shown above is the second-order result. The off-

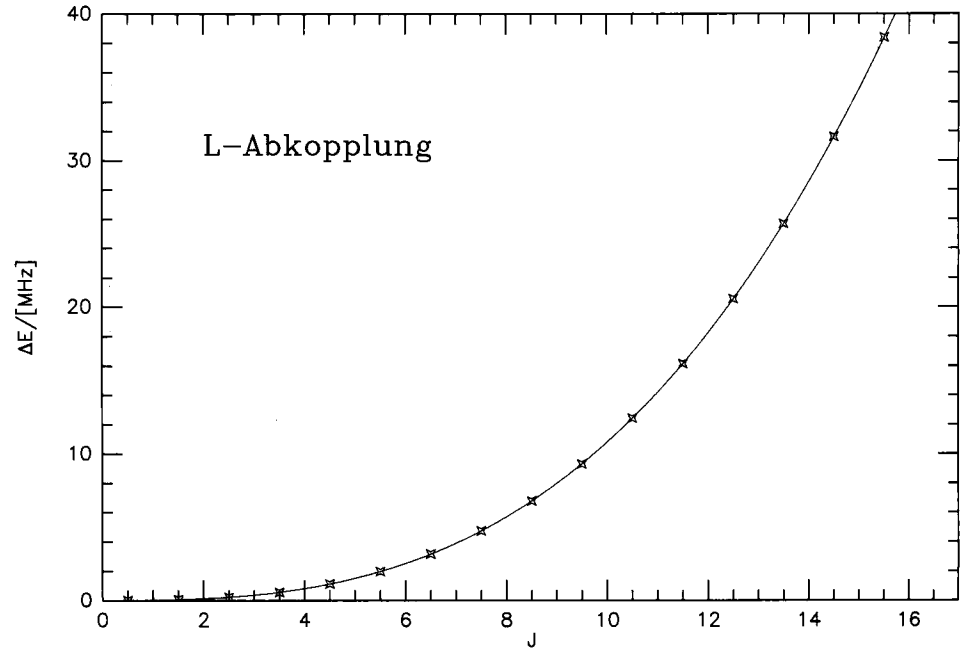

Figure 5. **L**-uncoupling in $N^{18}O$ is plotted versus J.

diagonal matrix elements of $(\hat{H}_{AD})$ are zero for molecules represented exactly by the parity basis of equation (6). Indeed, this holds for no molecule, since it requires a rotational constant of zero. When off-diagonal elements of $(\hat{H}_{AD})$ are included, the electron spin **S**, which is coupled to the orbital field of **L** in Hund's case (a) representation, will show a slight uncoupling due to admixture of Hund's case (d) in addition to its major uncoupling due to admixture of Hund's case (b). It can be stated in other words that while the linear Λ-type doubling in the $^2\Pi_{1/2}$ state is a pure measure of **L**-uncoupling, the Λ-type doubling in the $^2\Pi_{3/2}$ state is caused by a combination of **L**-uncoupling and **S** uncoupling. The additional uncoupling of **S** caused by case (d) admixture can be quantified by calculating the difference between the off-diagonal matrix elements between the $^2\Pi_{1/2}$ and $^2\Pi_{3/2}$ states in the presence and absence of matrix elements connecting the $^2\Pi$ and $^2\Sigma$ states. This difference is given by the off-diagonal elements in equation (12).

In figure 5, we have plotted the effect of the off-diagonal terms in the $(\hat{H}_{AD})$ matrix for $N^{18}O$ (which are solely responsible for any Λ-type doubling in the $^2\Pi_{3/2}$ substate) as a function of J. It can be seen that the effect, attributed to a combination of **L**-uncoupling and **S**-uncoupling, is much smaller than the effect of the **S**-uncoupling in case (b) depicted in figure 4, and that the J dependence is somewhat steeper, depending approximately on J^3. The ratio of the energetically split rotational terms of the $^2\Pi_{3/2}$ to the $^2\Pi_{1/2}$ fine structure term provides a qualitative measure of the joint effect of **L**-uncoupling and **S**-uncoupling compared with the pure uncoupling of **L**. This relation was calculated by first using the off-diagonal elements in equation (12), which represent the nonlinear contribution of the Λ-doubling causing (**L** + **S**)-uncoupling, and then by omitting the off-diagonal elements, yielding the pure **L**-uncoupling leading to Hund's case (d). In figure 6, these ratios are shown for the radicals NO, SH, and PS, all of which are of $^2\Pi$ symmetry. For the last molecule the ratio is extremely small so that the points are pictured on an enlarged scale by a factor of 50. Based on equations (11) and (12) light radicals with large rotational constants will show deviations from pure case (a) even at lower levels of J. For NO, the ratio of the rotational constant B to the fine structure constant A is roughly 0.01, so that even for a J as large as 14.5, the ratio of the Λ-type doubling in the $^2\Pi_{3/2}$ substate to the Λ-type doubling in the $^2\Pi_{1/2}$ substate is still only 10%. For PS, the ratio is $B/A = 0.0009$ and this radical approximates case (a) almost exactly, such that the analogous ratio is 0.2% at $J = 14.5$. The PS data were determined on the basis of measurements by Klein *et al.* [19] up to the 1 THz region. For SH [20, 21] the ratio is much larger, as pictured in figure 6, since $B/A = 0.025$. For a measure of the additional **S** uncoupling caused by admixture of Hund's case (d) compared with case (b), we have plotted in figure 7 the off-diagonal matrix elements in equation (12) divided by the off-diagonal matrix elements in equation (10) versus J for $N^{18}O$. The ratio is small and varies linearly with J.

Although we have been discussing uncoupling in terms of the quantum mechanical picture, it is also of use to discuss the semi-classical approach. In this

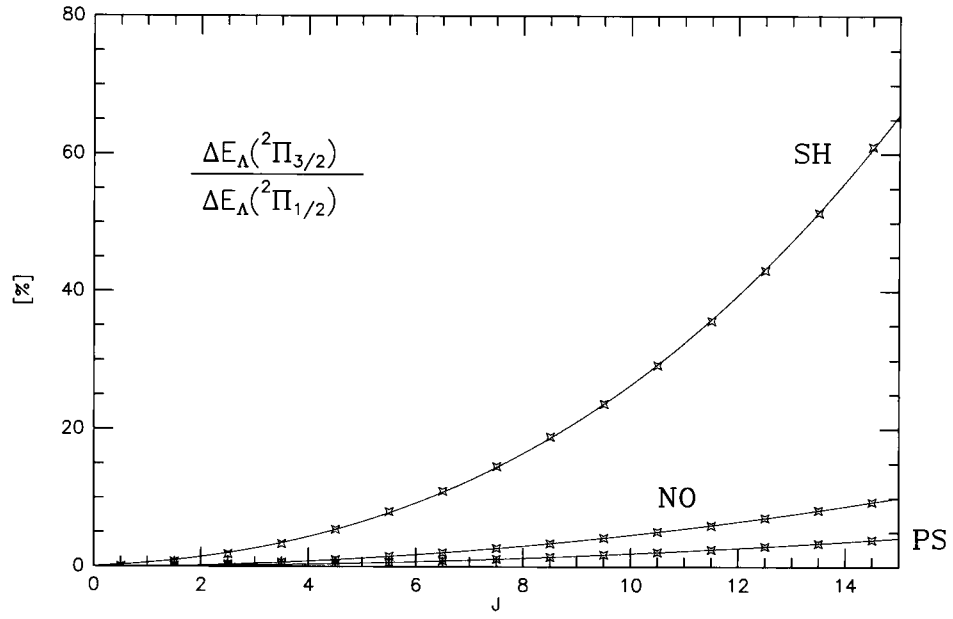

Figure 6. Ratio of the Λ-type doubling in the $^2\Pi_{3/2}$ state to that in the $^2\Pi_{1/2}$ state plotted as a function of J for the radicals NO, SH, and PS.

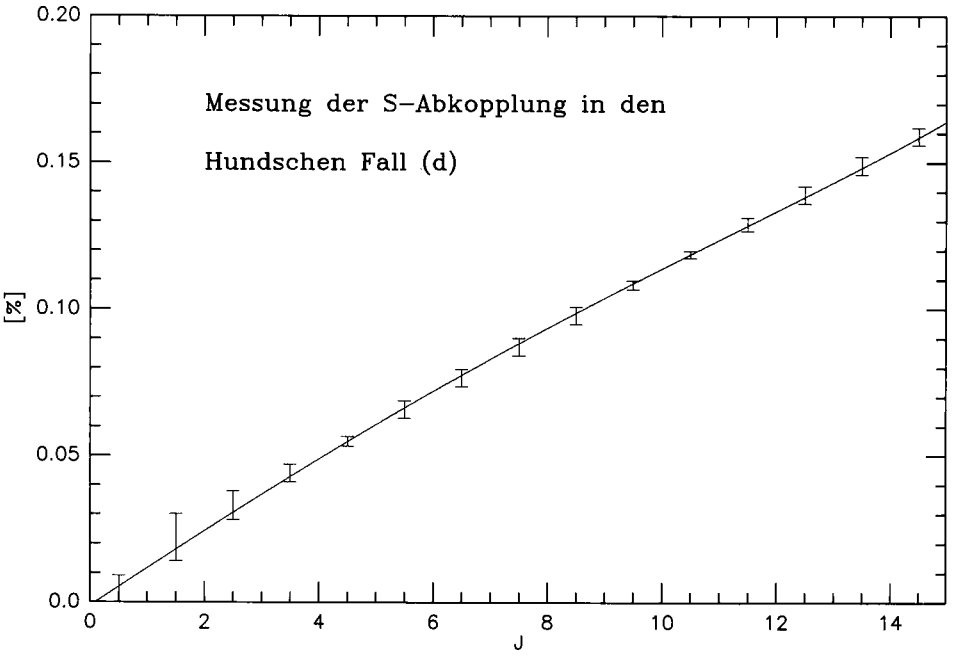

Figure 7. A measure of the extent of the additional S-uncoupling caused by the admixture of Hund's case (d) (via $^2\Sigma$ states) compared with the admixture of case (b) in $N^{18}O$ is plotted versus J. See text for a discussion of the measure.

picture, S-uncoupling and L-uncoupling are caused by inertial forces due to the molecular rotation: the electron spin **S** couples in Hund's case (b) via centrifugal forces—corresponding to the off-diagonal elements of the rotational parameter B in equation (10)—the angular momentum **L** via Coriolis forces [22] in Hund's case (d) (see also the appendix). The simultaneous nonlinear uncoupling of the electron spin **S** together with the angular momentum **L**+**S** in Hund's case (d) is a purely quantum mechanical effect and has no classical analogue. For molecules in good agreement with Hund's coupling scheme (a), such as PS, **S** and **L** are oriented parallel to the rotor axis. NO shows a similar behaviour only for the lower rotational states J, for which equations (11) and (12) are fulfilled; for higher J, a change into orthogonal planes is to be expected due to the different directions of centrifugal and Coriolis forces. The coupling of **S** and **L** in Hund's cases (b) and (d) deals with this aspect.

4.2. *Hyperfine structure*

The hyperfine splitting is dominated by the magnetic interactions between the nuclear spin **I** and the electronic orbital angular momentum **L** and spin **S**. These interactions exhibit a reverse behaviour from the Λ-doubling, in that the splittings are more pronounced in the $^2\Pi_{3/2}$ state.

The basis used for the hyperfine coupling corresponds to Hund's case (a_β), in which the nuclear spin **I** couples to **J** to form a resultant vector **F**. The diagonal hyperfine matrix elements (for the $I = 1/2$ case) in this basis used for the numerical fit are given by Brown [23] and Meerts [24]:

$$\begin{aligned}
&\langle {}^2\Pi_{\frac{1}{2}} J' \tfrac{1}{2} F \pm |\hat{H}_{\mathrm{Hfs}}| {}^2\Pi_{\frac{1}{2}} J \tfrac{1}{2} F \pm \rangle \\
&= G(I,J,J',F)\Bigg\{(-)^{J'-\frac{1}{2}}\begin{pmatrix} J' & 1 & J \\ -\frac{1}{2} & 0 & \frac{1}{2}\end{pmatrix}\left[a - \frac{b+c}{2}\right] \\
&\quad \pm (-)^{J-\frac{1}{2}}\begin{pmatrix} J' & 1 & J \\ \frac{1}{2} & -1 & \frac{1}{2}\end{pmatrix}\frac{d + \delta_{J,J'} X D_d}{2^{1/2}} \\
&\quad + 2\delta_{J,J'}(-)^{J'-\frac{1}{2}}\begin{pmatrix} J' & 1 & J \\ -\frac{1}{2} & 0 & \frac{1}{2}\end{pmatrix} X C_I\Bigg\} \\
&\quad + Q(I,J,J',F)(-)^{J'-\frac{1}{2}}\begin{pmatrix} J' & 2 & J \\ -\frac{1}{2} & 0 & \frac{1}{2}\end{pmatrix}\frac{eQq1}{4}, \qquad (13)
\end{aligned}$$

$$\begin{aligned}
&\langle {}^2\Pi_{\frac{3}{2}} J' \tfrac{1}{2} F \pm |\hat{H}_{\mathrm{Hfs}}| {}^2\Pi_{\frac{3}{2}} J \tfrac{1}{2} F \pm \rangle \\
&= G(I,J,J',F)(-)^{J'-\frac{3}{2}}\begin{pmatrix} J' & 1 & J \\ -\frac{3}{2} & 0 & \frac{3}{2}\end{pmatrix} \\
&\quad \times \left[a + \frac{b+c}{2} + \delta_{J,J'}\tfrac{2}{3} X C_I\right] \\
&\quad + Q(I,J,J',F)(-)^{J'-\frac{3}{2}}\begin{pmatrix} J' & 2 & J \\ -\frac{3}{2} & 0 & \frac{3}{2}\end{pmatrix}\frac{eQq_1}{4}, \qquad (14)
\end{aligned}$$

where

$$\begin{aligned}
G(I,J,J',F) &= (-)^{I+J'+F}[I(I+1)(2I+1)(2J+1) \\
&\quad \times (2J'+1)]^{1/2}\begin{pmatrix} F & J' & I \\ 1 & I & J\end{pmatrix}, \qquad (15)
\end{aligned}$$

$$\begin{aligned}
Q(I,J,J',F) &= (-)^{I+J'+F}\left(\frac{(I+1)(2I+1)(2I+3)}{I(2I-1)}\right. \\
&\quad \left.\times (2J+1)(2J'+1)\right)^{1/2}\begin{pmatrix} F & J' & I \\ 2 & I & J\end{pmatrix}, \qquad (16)
\end{aligned}$$

and the parameter D_d represents the hyperfine Λ-doubling. This small effect takes into account the distribution of the unpaired electron for the two Λ-doublet states and results in a magnetic hyperfine contribution. Note that the sign of the term containing the hyperfine-Λ-type doubling parameter d depends on the parity function.

The spin–rotation hyperfine interaction parameters C_I and $C_{I'}$ are of second order, as described by Townes and Schawlow [18], who reduce the effect to a perturbation caused by excited states with $\Delta\Lambda = \pm 1$; namely,

$$C_I \propto \sum \frac{\langle \Pi | r^{-3} L_+ | \Sigma \rangle \langle \Pi | B L_+ | \Sigma \rangle}{\Delta E}. \qquad (17)$$

The nuclear spin–rotation constants typically influence the hyperfine structure of molecules possessing strong bonding potential. For non-radicals, like HC_5N or other carbon chain molecules, the spin–rotation interaction C_I yields one contribution to the hyperfine structure. The magnetic hyperfine parameters a, b, and c cause a larger splitting for the $^2\Pi_{3/2}$ state than for the $^2\Pi_{1/2}$ state as a partial consequence of the different factors $[a - (b+c)/2]$ for $^2\Pi_{1/2}$ and $[a + (b+c)/2]$ for $^2\Pi_{3/2}$ in the diagonal matrix elements.

To understand this fully, one must look at the off-diagonal matrix elements, which are shown below:

$$\begin{aligned}
&\langle {}^2\Pi_{\frac{1}{2}} J' \tfrac{1}{2} F \pm |\hat{H}_{\mathrm{Hfs}}| {}^2\Pi_{\frac{3}{2}} J \tfrac{1}{2} F \pm \rangle \\
&= -G(I,J,J',F)(-)^{J'-\frac{3}{2}}\begin{pmatrix} J' & 1 & J \\ -\frac{3}{2} & 1 & \frac{1}{2}\end{pmatrix} \\
&\quad \times \frac{b \mp \delta_{J,J'}(J+\frac{1}{2}) C_I'}{2^{1/2}} \pm (-)^{J-\frac{1}{2}} Q(I,J,J',F) \\
&\quad \times \begin{pmatrix} J' & 2 & J \\ \frac{3}{2} & -2 & \frac{1}{2}\end{pmatrix}\frac{eQq_2}{96^{1/2}}. \qquad (18)
\end{aligned}$$

In these terms, the magnetic Fermi-contact interaction constant b and the electric quadrupole interaction eQq_2 represent the dominant contributions. Because the parameter b (see table 2) is rather small, the magnetic hyperfine interaction is dominated by diagonal contributions, but b affects the hyperfine spectrum due to the numerical diagonalization. In particular, the off-diagonal elements of b cause an increase of the hyperfine splitting of the $^2\Pi_{3/2}$ state and, vice versa, a decrease of the splitting of the $^2\Pi_{1/2}$ state. Since the Fermi contact interaction represents the non-vanishing probability of location of the unpaired electron near the nucleus, molecules with significantly larger hyperfine splitting in the $^2\Pi_{3/2}$ state than in the $^2\Pi_{1/2}$ state possess a higher

Table 3. Mean values of radial and spherical coordinates of the unpaired electron relative to the nitrogen nucleus.

	NO	^{15}NO	N^{18}O	Unit
$\langle r^{-3}\rangle_l$	14.752 53 (19)	14.753 70 (38)	14.754 2 (54)	$1 \cdot 10^{30}$ m^{-3}
$\langle r\rangle$	0.407 734 8 (18)	0.407 724 (35)	0.407 719 (50)	Å
$\langle r\rangle/r_e$	0.354 309 0 (16)	0.354 300 7 (35)	0.354 297 (43)	—
$\langle \sin^2(\Theta)\rangle$	0.891 345 (12)	0.891 280 (23)	0.891 108 (37)	—
$\langle \Theta\rangle$	70.75 (20)	70.75 (27)	70.7 (11)	degrees
$\lvert\psi_0\rvert^2$	0.466 43 (44)	0.468 80 (62)	0.469 (20)	$1 \cdot 10^{30}$ m^{-3}

probability that the unpaired electron density is large near the magnetic nucleus. The electric quadrupole hyperfine structure (see table 2) is dominated by the off-diagonal term, which contains the parameter eQq_2. This points to an uncoupling of the quadrupole tensor from the rotor axis.

All the magnetic hyperfine constants yield information about the electronic distribution [25]; in particular, a knowledge of a, b, c, and d can be used to determine $\langle r^{-3}\rangle$, where r is the distance of the unpaired electron from the N nucleus; $\langle \sin^2(\Theta)\rangle$, where Θ is the angle between the vector connecting the nucleus to the electron and the nuclear axis, and $|\psi_{(0)}|^2$, the probability for the electron to be located at the nucleus. The actual equations for these three parameters are as follows:

$$\langle r^{-3}\rangle_l = \frac{4 \times 10^6 \pi m_e m_p c^2}{e^2 \hbar} \frac{I}{\mu_I/\mu_N} a, \tag{19}$$

$$\langle \sin^2(\Theta) r^{-3}\rangle_s = \frac{16 \times 10^6 \pi m_e m_p c^2}{3 e^2 \hbar g} \frac{I}{\mu_I/\mu_N} d, \tag{20}$$

$$|\psi_{(0)}|^2 = \frac{3 \times 10^6 m_e m_p c^2}{e^2 \hbar g} \frac{I}{\mu_I/\mu_N} \left(b + \frac{c}{3}\right), \tag{21}$$

whereby the magnetic moment μ_I is given in nuclear magnetons and was taken from the IUPAC Commission on Atomic Weights and Isotopic Abundances [26]. The physical constants, proton and electron masses, m_p and m_e, the speed of light, c, the g-factor of the electron, g, the elemental charge, e, as well as Planck's constant, $\hbar$, including the experimental uncertainties of these constants [27], were used in calculating the mean values quoted in table 3.

The subscripts 'l' and 's' in the equations refer to the unpaired orbital and spin electron distributions, which need not be the same. A simple interpretation, however, is predicated on the assumption that the electron which contributes the orbital angular momentum is identical with that which contributes the spin momentum. Such a simplification is in accord with basic molecular orbital theory, in which the NO molecule possesses the following electronic ground state configuration [28]:

$$(\sigma_{1s})^2(\sigma_{1s}{}^*)^2(\sigma_{2s})^2(\sigma_{2s}{}^*)^2(\pi_{x,y})^4(\sigma_{2p})^2(\pi_{x,y}{}^*)^1, \tag{22}$$

where the * refers to an antibonding orbital. In this configuration, the unpaired electron, located in the antibonding π^* orbital, is indeed responsible for both the orbital and spin angular momentum. One can then argue that the first two equations refer to the same distribution and use them to infer values for $\langle r\rangle$ and $\langle \Theta\rangle$.

Table 3 contains a list of the parameters determined *directly* from the above equations for the three isotopomers studied, as well as some inferred parameters. The values can be used to characterize the unpaired electronic distribution. For example, the inferred value of $\langle r\rangle = 0.407$ Å represents about 35% of the equilibrium distance of $r_e = 1.150\,789\,3$ Å [4, 29, 30], showing that the electron is indeed closer to the N nucleus, as would be expected from the anti-bonding nature of the unpaired electron. Furthermore, $\langle \sin^2 \Theta\rangle = 0.891$ is in reasonable agreement with the value of 0.800 which pertains to a p_π electron in an atomic orbit about the nitrogen nucleus [18]. Yet, this electron cannot be said to be in a p orbital since it possesses some density at the N nucleus. Indeed, the probability that the free electron is located at the N nucleus, given by $|\psi_0|^2$, yields a value of 3.1% for the unpaired electron to be in a 2s atomic nitrogen state.

5. Interstellar aspects

Since the high frequency lines of NO reported here may be used by radio astronomers to study high-lying rotational states of this radical in interstellar space, it is instructive to discuss the interstellar chemistry and spectroscopy of NO. The NO radical in its ground $^2\Pi_{1/2}$ spin–orbit state has been detected in emission in several different environments in the interstellar medium [31–34]. The particular lines detected are the e–e and f–f components of the $J = 3/2$–$1/2$ transition, which lie between 150–151 GHz. These transitions have been observed both in cold dark interstellar clouds, which have temperatures $T \approx 10$ K and gas densities $\approx 10^4$ cm^{-3}, and in warmer regions ($T \approx 100$ K) surrounding newly forming stars. Depending on the specific

source detected, the 'fractional abundance' (mole fraction) of NO is on the order of 10^{-7}–10^{-8}. This relatively small value is explained quantitatively via standard treatments of the gas-phase chemistry [35, 36].

It is typically assumed that the initial form of the material in the gas phase of interstellar clouds is atomic, deriving from stellar ejecta, and that molecular synthesis then takes place mainly via gas-phase reactions that can occur efficiently at the low temperatures and densities of the interstellar gas [37]. Gas-phase chemistry is not the only possibility, however, because tiny dust particles also exist in interstellar clouds (size $\approx 0.1\,\mu m$) and chemical reactions can occur on their surfaces [37]. In particular, the dominant interstellar molecule, H_2, is formed only by association of two hydrogen atoms on the surfaces of dust particles. Once H_2 is desorbed into the gas, it is partially ionized by collisions with cosmic rays to form H_2^+, which in turn soon reacts with neutral hydrogen to form the triatomic ion H_3^+. This rudimentary polyatomic species can react with a variety of atoms to form a number of different molecular ions, which lead via complex series of ion–molecule, neutral–neutral, and recombination reactions, to many if not most interstellar molecules [37]. The radical NO is formed via one such chain of reactions.

The synthesis of NO commences with the reaction between H_3^+ and oxygen atoms, which leads to the OH^+ ion:

$$O + H_3^+ \rightarrow OH^+ + H_2. \tag{23}$$

This product ion is hydrogenated relatively quickly via reactions with molecular hydrogen to form the saturated H_3O^+ ion:

$$OH^+ + H_2 \rightarrow H_2O^+ + H, \tag{24}$$

$$H_2O^+ + H_2 \rightarrow H_3O^+ + H. \tag{25}$$

The rather stable hydronium ion does not react with H_2 but is neutralized via dissociative recombination reactions with electrons [38] in which the dominant oxygen-containing neutral product is the neutral hydroxyl radical. This radical is the direct precursor of NO, which is formed via the neutral–neutral reaction

$$N + OH \rightarrow NO + H; \tag{26}$$

the NO radical is subsequently destroyed by neutral reactions with atoms, such as

$$N + NO \rightarrow N_2 + O. \tag{27}$$

In addition to the NO radical, the nitrogen–oxygen chemical bond is also found in interstellar space in the interstellar molecules HNO and N_2O [39].

6. Summary

The molecular parameters for the ground electronic state of three isotopomers of the NO radical have been determined with high accuracy, as listed in table 2, and are in good agreement with those in the literature. These parameters include rotational and spin–orbit constants, fine-structure parameters related to the Λ-doubling, and a complete set of hyperfine parameters for the magnetic dipole, electric quadrupole, and spin–rotation interactions. The spin–orbit parameter A and its centrifugal distortion term D_A were obtained through the inclusion of the magnetic dipole transitions ($^2\Pi_{3/2} \leftarrow {}^2\Pi_{1/2}$) [5], while the spin–rotation parameter γ was set equal to zero, because its matrix elements are dependent on those of D_A. For $^{14}N^{16}O$ and $^{14}N^{18}O$, an accurate fit to the 1 THz spectroscopic data requires the inclusion of the higher-order rotational centrifugal correction parameter H. The complete set of hyperfine parameters for the $^{14}N^{18}O$ isotopomer has been determined for the first time. We have examined the details of the intermediate coupling case of NO due to **S**- and **L**-uncoupling via the rotational motion, whereby quantum mechanical perturbation calculations prove to be similar to a treatment of artificial forces in the classical picture. Moreover, we have presented an accurate calculation of the unpaired electron density, from which the radial and spherical coordinates of the unpaired electron around the nitrogen atom were determined. We note, finally, that our measurements of NO transitions with extremely low intensities provide an excellent demonstration of the quality of our 1 THz spectrometer.

The authors thank A. Dolgner for preparing the NO samples. E.H. and G.W. thank the Max-Planck-Gesellschaft and Alexander-von-Humboldt-Stiftung for the Max Planck Research Award. The work in Köln was supported in part by the Deutsche Forschungsgemeinschaft (DFG) via grant SFB 301 and special funding from the Science Ministry of the Land Nordrhein-Westfalen. The work of S.P.B. at Köln was made possible by the DFG through grants aimed to support Eastern and Central European countries and the republics of the former Soviet Union.

Appendix

In the classical picture, the different uncoupling effects of electronic spin **S** and orbital angular momentum **L** from the rotor axis can be described by inertial forces due to the molecular rotation. First we show that the angular momentum vector **L** is uncoupled from the rotor axis by the Coriolis force:

$$\mathbf{F}_{Cor} = 2m\mathbf{v} \times \omega, \tag{A 1}$$

where m is the electronic mass, $\mathbf{v}$ is the electronic velocity relative to the rotating frame, and ω is the angular velocity of the rotating molecule. To deduce a velocity-dependent potential for the Coriolis force, it is convenient to make an analogy with electromagnetism. In the case of electric and magnetic fields $\mathbf{E}$ and $\mathbf{B}$, a charged particle is affected by the Lorentz force:

$$\mathbf{F}_{(\mathbf{r},\mathbf{v},t)} = q\left(\mathbf{E}_{(\mathbf{r},t)} + \frac{\mathbf{v}}{c} \times \mathbf{B}_{(\mathbf{r},t)}\right). \tag{A 2}$$

On the basis of Maxwell's equations, the electric and magnetic fields can be expressed by the scalar and vector potential $\phi_{(\mathbf{r},t)}$ and $\mathbf{A}_{(\mathbf{r},t)}$ as

$$\mathbf{B}_{(\mathbf{r},t)} = \nabla \times \mathbf{A}_{(\mathbf{r},t)}, \tag{A 3}$$

$$\mathbf{E}_{(\mathbf{r},t)} = -\nabla\phi_{(\mathbf{r},t)} - \frac{1}{c}\dot{\mathbf{A}}_{(\mathbf{r},t)}. \tag{A 4}$$

The Hamilton function in this case is well known to be

$$\mathbf{H}_{(\mathbf{q},\mathbf{p},t)} = \frac{1}{2m}\left(\mathbf{p} - \frac{e}{c}\mathbf{A}\right)^2 + e\phi. \tag{A 5}$$

Equation (A 5) is analogous to the Coriolis case if we take

$$\omega = \frac{e}{2mc}\nabla \times \mathbf{A} \Rightarrow \mathbf{A} = \frac{mc}{e}(\omega \times \mathbf{r}), \tag{A 6}$$

the scalar potential ϕ is set to zero due to the absolute magnetic attribute of fine structure transitions and therefore **L**-uncoupling transitions. It should be of the order of the coefficient mc/e in the vector potential $\mathbf{A}$ which ranges of the size 10^0 and thus refers to classical scale. The Hamilton function for the Coriolis case is then given by

$$\mathbf{H}_{(\mathbf{q},\mathbf{p},t)} = \frac{1}{2m}\{\mathbf{p} - m(\omega \times \mathbf{r})\}^2 \tag{A 7}$$

$$= \frac{1}{2m}\{p^2 - 2m\mathbf{p}(\omega \times \mathbf{r}) + m^2(\omega \times \mathbf{r})^2\} \tag{A 8}$$

$$\approx \frac{p^2}{2m} - \mathbf{p}(\omega \times \mathbf{r}) + \mathcal{O}^2_{(\mathbf{r})} \tag{A 9}$$

$$= \frac{p^2}{2m} + \underbrace{(\mathbf{p} \times \mathbf{r})}_{-\mathbf{L}}\omega, \tag{A 10}$$

where $\mathcal{O}^2_{(r)}$ represents higher-order terms and $\mathbf{L} = \mathbf{r} \times \mathbf{p}$ is the angular momentum of the electron. Using the classical relation $\mathbf{R} = \Theta\omega$ and taking into account that the moment of inertia for diatomic molecules is $\Theta \sim 1/2B$, we obtain the final form of the Hamilton function:

$$\mathbf{H}_{(\mathbf{q},\mathbf{p},t)} = \frac{p^2}{2m} - 2\mathbf{BL}\cdot\mathbf{R}, \tag{A 11}$$

where $\mathbf{R}$ is the rigid-body rotational momentum of the molecule. The first term of equation (A 11) describes the standard electronic motion whereas the second term, originating from the Coriolis force, represents the interaction of the electronic orbital angular momentum $\mathbf{L}$ with the molecular rotation $\mathbf{R}$, which couples $\mathbf{L}$ to the rigid body rotational angular momentum, as in case (d). It should be noted that our semi-classical derivation of **L**-uncoupling on the basis of Coriolis forces results in a negative sign (A 11), which is in line with the defined expression of Judd (see [22], equation (9.4)). The negative sign refers to the uncoupling direction of $\mathbf{L}$ away from the nuclear axis.

In a similar manner, the **S**-uncoupling effect can be treated by considering the centrifugal force of an individual electron of mass m:

$$\mathbf{F}_{\text{Cen}} = m\{\omega \times (\mathbf{r} \times \omega)\} \tag{A 12}$$

$$= m\left\{\mathbf{r}\omega^2 - \omega\underbrace{(\omega\mathbf{r})}_{=0}\right\} = m\omega^2\mathbf{r}. \tag{A 13}$$

The term $\omega\mathbf{r}$ is set to zero because the angular momentum of the end-over-end molecular rotation points perpendicular to the molecular axis. Thus the centrifugal force is conservative and a scalar 'effective' potential can be obtained:

$$\mathbf{F} = -\nabla U \Rightarrow U = -\tfrac{1}{2}m\omega^2 r^2. \tag{A 14}$$

The Hamilton function for electronic motion is then given by

$$\mathbf{H}_{(\mathbf{q},\mathbf{p},t)} = \frac{p^2}{2m} - \tfrac{1}{2}mr^2\omega^2, \tag{A 15}$$

where the first term is its kinetic energy in the absence of molecular rotation. The relations $mr^2 = \Theta \sim 1/2B$ and $\omega^2 = R^2/\Theta^2 \sim 4B^2R^2$ lead to

$$\mathbf{H}_{(\mathbf{q},\mathbf{p},t)} = \frac{p^2}{2m} - \mathrm{BR}^2. \tag{A 16}$$

Obviously, the electron spin $\mathbf{S}$ cannot be replaced by any classical momentum because $\mathbf{S}$ is a purely quantum mechanical operator. Still, the additional term in equation (A 16) caused by the rotational motion is equivalent to the effect of **S**-uncoupling in equation (10), where the magnitude of the effect is determined by off-diagonal matrix elements depending on B and J. Once again, the sign of the **S**-uncoupling turns out to be negative (A 16).

It is interesting to note that on the basis of classical mechanics both **L** and **S** uncoupling, which are normally treated by a second-order-perturbation quantum mechanical procedure, are caused by fictional forces in a non-inertial frame. Both effects are proportional to the rotational parameter B.

References

[1] HUND, F., 1926, *Z. Phys.*, **36,** 657.

[2] HERZBERG, G., 1950, *Molecular Spectra and Molecular Structure I: Spectra of Diatomic Molecules* (New York: Van Nostrand).

[3] BERINGER, R., and CASTLE, J. G., 1950, *Phys. Rev.*, **78,** 581.

[4] SALECK, A. H., YAMADA, K. M. T., and WINNEWISSER, G., 1991, *Molec. Phys.*, **72,** 1135.

[5] SALECK, A. H., WINNEWISSER, G., and YAMADA, K. M. T., 1992, *Molec. Phys.*, **76,** 1443.

[6] SALECK, A. H., LIEDTKE, M., DOLGNER, A., and WINNEWISSER, G., 1994, *Z. Naturforsch.*, **49a,** 1111.

[7] WINNEWISSER, G., 1995, *Vib. Spectrosc.*, **8,** 241.

[8] WINNEWISSER, G., BELOV, S. P., KLAUS, TH., and SCHIEDER, R., 1997, *J. molec. Spectrosc.*, **184,** 468.

[9] HOFMANN, K. A., and HOFMANN, U. R., 1941, *Lehrbuch der Anorganischen Chemie.*

[10] GORDY, W., and COOK, R. L., 1984, *Microwave Molecular Spectra, Techniques of Chemistry*, Vol. XVIII, 3rd Edn (New York: Wiley).

[11] BROWN, J. M., HOUGEN, J. T., HUBER, K. P., JOHNS, J. W. C., KOPP, L., LEFEBVRE-BRION, H., MERER, A. M., RAMSAY, D. A., ROSTAS, J., and ZARE, R. N., 1975, *J. molec. Spectrosc.*, **55,** 500.

[12] BELOV, S. P., YAMADA, K. M. T., WINNEWISSER, G., PLOTEAU, L., BOCQUET, R., DEMAISON, J., POLYANSKI, O., and TRETYAKOV, YU., 1995, *J. molec. Spectrosc.*, **173,** 380.

[13] MEERTS, W. L., and DYMANUS, A., 1972, *J. molec. Spectrosc.*, **44,** 320.

[14] MEERTS, W. L., 1976, *Chem. Phys.*, **14,** 421.

[15] ZARE, R. N., SCHMELTEKOPF, R. J., HARROP, W. J., and ALBRITTON, D. L., 1973, *J. molec. Spectrosc.*, **46,** 37.

[16] CARRINGTON, A., 1974, *Microwave Spectroscopy of Free Radicals* (London: Academic Press).

[17] VAN VLECK, J. H., 1932, *The Theory of Electric and Magnetic Susceptibilities* (London: Oxford University Press).

[18] TOWNES, C. H., and SCHAWLOW, A. L., 1955, *Microwave Spectroscopy* (New York: Dover Publications, Inc.).

[19] KLEIN, H., KLISCH, E., and WINNEWISSER, G., 1999, *Z. Naturforsch.* **54a,** 137.

[20] KLISCH, E., KLAUS, TH., BELOV, S. P., WINNEWISSER, G., and HERBST, E., 1996, *Amazing Light*, edited by R. Y. Chiao (New York: Springer), p. 355.

[21] KLISCH, E., KLAUS, TH., BELOV, S. P., DOLGNER, A., SCHIEDER, R., WINNEWISSER, G., and HERBST, E., 1996, *ApJ.*, **473,** 1118.

[22] JUDD, B. R., 1975, *Angular Momentum Theory for Diatomic Molecules* (New York: Academic Press).

[23] BROWN, J. M., KAISE, M., KERR, C. M. L., and MILTON, D. J., 1978, *Molec. Phys.*, **36,** 553.

[24] MEERTS, W. L., BEKOOY, J. P., and DYMANUS, A., 1979, *Molec. Phys.*, **37,** 425.

[25] FROSCH, R. A., and FOLEY, H. M., 1952, *Phys. Rev.*, **88,** 1337.

[26] INTERNATIONAL UNION OF PURE AND APPLIED CHEMISTRY, IUPAC, 1988, *Quantities, Units, and Symbols in Physical Chemistry* (Oxford: Alden Press).

[27] 1987, *Phys. Bl.*, **43.**

[28] CAMPBELL, J. A., 1970, *Chemical Systems, Energetics, Dynamics, and Structure* (San Francisco, London: W. H. Freeman and Company).

[29] VAN DEN HEUVEL, F. C., MEERTS, W. L., and DYMANUS, A., 1980, *J. molec. Spectrosc.*, **84,** 162.

[30] AMIOT, C., BACIS, R., and GUELACHVILI, G., 1978, *Can. J. Phys.*, **56,** 251.

[31] MCGONAGLE, D., IRVINE, W. M., MINH, Y. C., and ZIURYS, L. M., 1990, *Astrophys. J.*, **359,** 121.

[32] GERIN, M., VIALA, Y., PAUZAT, F., and ELLINGER, Y., 1992, *Astron. Astrophys.*, **266,** 463.

[33] ZIURYS, L. M., MCGONAGLE, D., MINH, Y. C., and IRVINE, W. M., 1991, *Astrophys. J.*, **373,** 535.

[34] GERIN, M., VIALA, Y., and CASOLI, F., 1993, *Astron. Astrophys.*, **268,** 212.

[35] LEE, H. H., BETTENS, R. P. A., and HERBST, E., 1996, *Astron. Astrophys.*, **119** (Suppl.), 111.

[36] MILLAR, T. J., FARQUHAR, P. R. A., and WILLACY, K., 1997, *Astron. Astrophys.*, **121,** 139.

[37] HERBST, E., 1995, *Ann. Rev. Phys. Chem.*, **46,** 27.

[38] VEJBY-CHRISSTENSEN, L., ANDERSEN, L. H., HEBER, O., KELLA, D., PEDERSEN, H. B., SCHMIDT, H. T., and ZAIFMAN, D., 1997, *Astrophys. J.*, **483,** 531.

[39] ZIURYS, L. M., APPONI, A. J., HOLLIS, J. M., and SNYDER, L. E., 1994, *Astrophys. J.*, **436,** L181.